Effects of primary particle diameter and aggregate size distribution on the temperature of soot particles heated by pulsed lasers

Liu, Fengshan; Smallwood, Gregory J.; Snelling, David R.

Publisher's version / Version de l'éditeur:
https://doi.org/10.1016/j.jqsrt.2004.08.027
Journal of Quantitative Spectroscopy & Radiative Transfer, 93, June, pp. 301-312, 2005

MARIA CLANCY
DGO
INST FOR CHEM PROCESS & ENVIR TECH
NATIONAL RESEARCH COUNCIL CANADA
M-12, ROOM 141, 1200 MONTREAL RD.
OTTAWA, ON K1A 0R6
CANADA

ORDER NUMBER:	**CI-07780893-6**
Account Number:	WR001844
Delivery Mode:	XLB
Delivery Address:	
Submitted:	2009/03/03 10:39:15
Received:	2009/03/03 10:39:15
Printed:	2009/03/03 21:07:08

Extended	**Periodical**	**Virtual Lib. Blank form**	**CANADA**

Client Number:	MARIA E. CLANCY
Title:	**JOURNAL OF QUANTITATIVE SPECTROSCOPY AND RADIATIVE TRANSFER**
Vol./Issue:	93
Date:	2005
Pages:	301-312
Article Title:	PRIMARY PARTICLE DIAMETER AND AGGREGATE SIZE DISTRIBUTION ON THE TEMPERATURE OF SOOT PARTICLES HEATED BY PULSED LASERS
Article Author:	LIU, F.; SMALLWOOD, G.J.; SNELLING, D.R.

INSTRUCTIONS: NEEDED BY: 31 MARCH 2009

Estimated cost for this 12 page document: $0 document supply fee + $0 copyright = $0

ELSEVIER

Journal of Quantitative Spectroscopy & Radiative Transfer 93 (2005) 301–312

Journal of Quantitative Spectroscopy & Radiative Transfer

www.elsevier.com/locate/jqsrt

Effects of primary particle diameter and aggregate size distribution on the temperature of soot particles heated by pulsed lasers

Fengshan Liu*, Gregory J. Smallwood, David R. Snelling

Combustion Technology Group, Institute for Chemical Process and Environmental Technology, National Research Council, Building M-9, 1200 Montreal Road, Ottawa, Ont., Canada K1A 0R6

Received 1 February 2004; accepted 1 July 2004

Abstract

Temperature histories of nanosecond-pulsed laser-heated soot particles of different primary particle diameters and different aggregate sizes were calculated using an aggregate-based heat transfer model. Relatively low laser fluences were considered to ensure maximum particle temperatures were below about 3800 K to avoid soot particle sublimation. After the laser pulse, the temperature of soot particles in larger aggregates decreases more slowly than that of particles in smaller aggregates due to the increased shielding effect. For a given aggregate size, the temperature of particles of smaller diameter decays faster as a result of a larger surface area-to-volume ratio. The effective temperature of soot particles in the laser probe volume was calculated based on the ratio of thermal radiation intensities of soot particles at 400 and 780 nm to simulate the experimentally measured soot particle temperature using two-color optical pyrometry. The effect of aggregate size distribution of soot particles on the effective particle temperature was investigated under different initial temperatures.

Keywords: Laser induced incandescence; Radiation based diagnostic; Nanoparticle heat transfer

*Corresponding author. Tel.: +1-613-993-9470; fax: +1-613-957-7869.
E-mail address: fengshan.liu@nrc-cnrc.gc.ca (F. Liu).

0022-4073/$ - see front matter
doi:10.1016/j.jqsrt.2004.08.027

1. Introduction

Optical diagnostic techniques play an important role in our understanding of soot formation, growth, aggregation, and oxidation in flames and in characterizing the morphology of nanoparticles such as soot, diesel particulate matter, and carbon black. While traditional techniques can provide information on soot characteristics including soot volume fraction by laser extinction [1] and soot morphology (primary particle diameter and aggregate size distribution) by laser scattering [2] and thermophoretic sampling/transmission electron microscopy analysis (TS/TEM) [3], they suffer various limitations compared to the more recently developed laser-induced incandescence (LII) technique [4–7]. LII has been proven to be a useful diagnostic tool for spatially and temporally resolved measurement of soot volume fraction and primary particle size in a wide range of applications. To date the LII technique can provide soot volume fraction and primary soot particle diameter [8], but cannot provide information on aggregate size distribution.

A practical method to measure the surface temperature of particles (soot, coal, and carbon) is optical pyrometry, based on the particle thermal emission intensities detected at two or more wavelengths. When the temperature of soot particles in the measurement volume is non-uniform, the measured temperature is an *effective temperature*, which is a weighted average temperature. Various optical pyrometers have also been used to monitor the soot particle temperature during LII. Eckbreth [9] measured the laser-irradiated soot particle surface temperatures using the LII signals detected at two different wavelengths. Snelling et al. [8] employed a three-wavelength pyrometer to measure the laser-heated soot particle surface temperatures in a diesel engine exhaust.

Theoretical models describing the nanoscale heat and mass transfer processes of LII have been developed and improved over the last two decades [10,11 and references cited therein]. However, significant uncertainty may still exist in the numerical results under conditions of significant soot sublimation primarily due to the lack of reliable physical parameters in the soot sublimation sub-model such as the vapor pressure and the heat of vaporization [12]. To avoid the uncertainty in the sublimation sub-model in numerical study and to make the LII technique truly non-intrusive, our recent experimental and numerical studies [13] have focused on low-fluence LII, in which the maximum soot particle temperature remains below about 3800 K, ensuring negligible soot sublimation. Besides the uncertainty in the sublimation sub-model, which can be avoided by using a low-fluence laser beam, the accuracy of the primary soot particle diameter estimated using the experimental temperature decay rate [8] is severely limited by our knowledge of the soot particle thermal accommodation coefficient α. The values for α of soot particles cited in the literature is subjected to significant uncertainty, from 0.26 [7] to 0.9 [14]. Our recent study has determined new values of soot absorption function $E(m)$ at 1064 nm and the soot particle thermal accommodation coefficient α based on experimental temperature decay rate and known soot morphology in a laminar diffusion flame [13]. Except for our recent study [13], in which an attempt was made to formulate a more realistic aggregate-based LII model, to our knowledge all the theoretical models of LII appearing in the literature were developed for a single primary particle.

Soot particles in general appear as mass-fractals as a result of aggregation [2,3,15] rather than isolated primary particles. Therefore, the mass-fractal structure of soot particles should be taken into account in the LII model. The fractal structure of soot aggregates results in a *shielding effect* for heat conduction between the soot aggregates and the surrounding gas, as some primary particles are partially or fully hidden from the exterior of the aggregate. The shielding effect

reduces the available surface area of the soot particles for collision with the surrounding gas molecules. As a result, soot particles in larger aggregates have a slower cooling rate than those in smaller aggregates. Therefore, even though heated to the same peak temperature, soot particles exhibit different temperatures at later times after the laser pulse.

In this study numerical calculations were conducted to obtain the temperature history of soot particles in aggregates of different sizes. Assuming the aggregate size distribution is log-normal, the effective temperature of soot particles in the laser probe volume was calculated based on the ratio of thermal emission intensities of soot particles at 400 and 780 nm to simulate the experimentally measured soot particle temperature using two-color optical pyrometry. The objectives of the present study are (i) to further improve the current LII model by using an improved sub-model for heat conduction between soot aggregates and the surrounding gas, and (ii) to investigate the effect of aggregate size distribution on the temporal decay rate of the effective soot temperature. The present study demonstrates that the temporal decay rate of soot particle temperature after the laser pulse depends not only on the primary soot particle diameter but also on the aggregate size, in terms of the number of primary particles per aggregate. Through such an improved understanding of the temporal decay rate of the effective soot particle temperature determined by two-color optical pyrometry, it is concluded that the temporal decay rate of soot particle temperature alone is, in general, insufficient to determine the primary soot particle diameter.

2. Theory

2.1. Low-fluence LII model

Soot particles in general form fractal-like structures (aggregates) with some bridging between the primary particles [2,3,15]. However, it is a reasonable approximation to model soot aggregates as monodisperse spherical primary particles that are just in point contact [15]. Although the laser energy absorption rate of soot particles is not affected by aggregation based on results from Rayleigh–Debye–Gans polydisperse fractal aggregate (RDG-PFA) theory [2,15], the heat loss rate of soot particles to the surrounding gas, primarily through heat conduction, is dependent on the aggregate size as a result of the shielding effect. The shielding effect not only reduces the heat transfer rate per unit surface area of soot particle but also potentially causes a non-uniform temperature distribution within an aggregate after the laser pulse. As a first approximation, however, the non-uniformity in temperature distribution within an aggregate is not taken into account, i.e. it is assumed that all the primary soot particles within an aggregate have the same temperature.

The aggregate-based LII model described in Ref. [13] was improved by incorporating a more accurate model to calculate the rate of heat conduction between the soot aggregate and the surrounding gas in the transition regime. In the absence of soot sublimation, the energy conservation equation of a soot aggregate can be written as

$$\frac{1}{6}\pi d_{\mathrm{p}}^{3} N_{\mathrm{p}} \rho_{\mathrm{s}} c_{\mathrm{s}} \frac{\mathrm{d}T}{\mathrm{d}t} = C_{\mathrm{a}} F_{0} q(t) N_{\mathrm{p}} - \dot{q}_{\mathrm{c}} - \dot{q}_{\mathrm{r}}. \tag{1}$$

In Eq. (1) d_p is the primary soot particle diameter (typically between 20 and 50 nm), N_p the aggregate size (number of primary particles per aggregate), ρ_s and c_s are soot particle density and specific heat, and T and t are soot particle temperature and time, respectively. On the right-hand side of Eq. (1), $C_a = \pi^2 d_p^3 E(m)/\lambda$ is the absorption cross section of a primary soot particle in the Rayleigh limit. In this study, the laser wavelength λ is 1064 nm. F_0 is the laser fluence in mJ/mm^2. Function $q(t)$ is the pulsed-laser temporal power density per unit laser fluence (mJ/mm^2). Symbols $\dot{q}_c$ and $\dot{q}_r$ represent, respectively, the rate of conduction heat loss from the aggregate to the surrounding gas and radiation heat loss rate. Although conduction heat loss is the dominant particle heat loss, the heat loss due to radiation is nevertheless included in this study. Again, radiation heat loss is not affected by particle aggregation based on the RDG-PFA theory and can be written as

$$\dot{q}_r = N_p \int_0^\infty \frac{2\pi c^2 h}{\lambda^5} \frac{1}{\exp(hc/k_B \lambda T) - 1} \pi d_p^2 \frac{4\pi d_p E(m)}{\lambda} \mathrm{d}\lambda, \tag{2}$$

where symbols h, k_B and c represent the Planck constant, the Boltzmann constant, and the speed of light, respectively. The soot absorption function $E(m)$ is in general dependent on the wavelength in the visible and the infrared. Since heat loss due to thermal emission from soot particles is much smaller than that due to heat conduction, an average value of $E(m)$ was used in the evaluation of the above integration. After some derivation, Eq. (2) can be written as

$$\dot{q}_r = 8\pi^3 d_p^3 \bar{E}(m) \frac{k_B^5}{h^4 c^3} T^5 N_p \int_0^\infty \frac{t^4}{e^t - 1} \mathrm{d}t, \tag{3}$$

where the integration yields a value of 24.886 and an average value of 0.4 is assigned to $\bar{E}(m)$.

Calculation of the rate of conduction heat loss can be described in two steps. First, the mass-fractal structure of soot aggregates needs to be approximately represented by an equivalent sphere which has the same effective surface area as far as heat conduction with the surrounding gas is concerned. For this purpose, the aggregate projected area-based equivalent sphere model described in our previous study [13] was used. In this model, the diameter of the equivalent sphere is related to the primary soot particle diameter d_p and the aggregate size N_p through [13]

$$D_a = \left(\frac{N_p}{f_a}\right)^{1/2\varepsilon_a} d_p, \tag{4}$$

where f_a and ε_a are respectively prefactor and exponent for the aggregate project area. It should be noted that the correlation relationship in Eq. (4) does not hold for $N_p = 1$; in this case D_a is simply set to d_p. Different values of f_a and ε_a have been suggested in the literature based on experimental measurements [16] and numerical simulation [17]. In the present calculation, the values of $f_a = 1.1$ and $\varepsilon_a = 1.08$, recommended by Brasil et al. [17], based on numerically generated aggregates were employed. The numerical simulation of aggregates in [17] was based on values of the fractal parameters D_f and k_g of 1.78 and 1.5, respectively. The relation between aggregate size N_p and the radius of gyration R_g is given by

$$N_p = k_g \left(\frac{R_g}{d_p/2}\right)^{D_f}. \tag{5}$$

Köylü et al. [18] have compared their experimental results with others and concluded that for all the data and all types of flames $D_f = 1.7 \pm 0.15$ and $k_g = 2.4 \pm 0.4$. The fractal prefactor assumed in [17] is somewhat outside these error limits but the fractal dimension is in agreement.

Once a heat conduction equivalent sphere is properly defined, the next step is to calculate the heat conduction rate between the equivalent sphere and the surrounding gas in the transition regime. In this work, instead of using the simple harmonic mean expression for conduction heat transfer rate in the transition regime employed in our previous study [13], we used the Fuch's approach based on a recent study of Filippov and Rosner [19] who showed that the simple harmonic mean method can give rise to significant errors under large particle-to-gas temperature ratios such as in the case of laser-heated carbon black particles initially at room temperature. The key to this approach is to find the radius and temperature of a limiting sphere, which is larger than the heat transfer equivalent sphere described above, Eq. (4). The limiting sphere is defined as such that inside the sphere the heat conduction is in the free-molecular regime (between particle temperature T and the limiting sphere temperature T_δ) and outside it the heat conduction is in the continuum regime (between the gas temperature T_g and the limiting sphere temperature T_δ). Inside the limiting sphere the heat conduction rate from the equivalent sphere to the region within the limiting sphere is calculated using the free-molecular regime expression as [19]

$$\dot{q}_c = \alpha\pi R_a^2 \frac{p_g}{2}\sqrt{\frac{8k_B T_\delta}{\pi m_g}}\frac{\gamma^* + 1}{\gamma^* - 1}\left(\frac{T}{T_\delta} - 1\right), \tag{6}$$

where α is the soot particle thermal accommodation coefficient, R_a is the radius of the equivalent sphere ($D_a/2$), p_g is the gas pressure, k_B is the Boltzmann constant, m_g the mass of the gas molecule, and γ^* the average value of the specific heat ratio defined as

$$\frac{1}{\gamma^* - 1} = \frac{1}{T - T_\delta}\int_{T_\delta}^{T}\frac{\mathrm{d}T}{\gamma - 1}. \tag{7}$$

In the region outside the limiting sphere the conduction heat loss from the limiting sphere to the surrounding gas is calculated using the continuum regime expression as [19]

$$\dot{q}_c = 4\pi(\delta + R_a)\int_{T_g}^{T_\delta} k_g\,\mathrm{d}T, \tag{8}$$

where δ is the thickness of the boundary layer in the Fuch's approach, i.e. $\delta + R_a$ is the radius of the limiting sphere, k_g is the conduction coefficient of the surrounding gas. The ratio of radius of the limiting sphere to the equivalent sphere is given as [19]

$$\frac{\delta + R_a}{R_a} = \frac{R_a^2}{\lambda_\delta^2}\left(\frac{1}{5}\Lambda_1^5 - \frac{1}{3}\Lambda_2\Lambda_1^3 + \frac{2}{15}\Lambda_2^{5/2}\right), \tag{9}$$

where λ_δ is the mean free path of gas molecules in the boundary layer around the equivalent sphere and Λ_1 and Λ_2 are given as

$$\Lambda_1 = 1 + \lambda_\delta/R_a, \quad \Lambda_2 = 1 + (\lambda_\delta/R_a)^2. \tag{10}$$

Using the expression given by McCoy and Cha [20] the mean free path can be calculated as

$$\lambda_g = \frac{k_g(T_g)}{fp_g}(\gamma - 1)\sqrt{\frac{\pi m_g T_g}{2k_B}}, \tag{11}$$

where f is the Eucken factor [21]. The mean free path in the limiting sphere is related to that in the surrounding gas through

$$\lambda_\delta = \frac{k_g(T_\delta)}{k_g(T_g)}\sqrt{\frac{T_\delta}{T_g}}\lambda_g. \tag{12}$$

Once the boundary layer thickness δ and the temperature in the limiting sphere T_δ are obtained by solving Eqs. (6)–(12) iteratively, the conduction heat loss rate can be calculated using either Eq. (6) or Eq. (8).

2.2. Effective particle temperature

When the temperature of soot particles in the laser probe volume is non-uniform, two-color optical pyrometry provides a weighted average or effective particle temperature. In the present study, we consider a uniform spatial laser energy profile and the non-uniformity in soot particle temperature is due to the aggregate size-dependent heat conduction process. Once the history of soot particle temperatures is obtained for a range of aggregate sizes N_p by solving Eq. (1), the numerically simulated total LII signals detected at two different wavelengths in the near-visible (400 and 780 nm) can be obtained by integrating the thermal emission intensity of soot particles over the entire aggregate size range assuming some aggregate size distribution function.

Assuming soot particles are uniformly distributed inside the laser probe volume and the probe volume is small enough to ensure that the optically thin assumption is valid, the total thermal emission intensity (TEI) at a wavelength λ_i is

$$TEI_i \propto \int_1^\infty p(N_p)N_p \frac{2\pi c^2 h}{\lambda_i^5}\left[\exp\left(\frac{hc}{\lambda_i k_B T}\right) - 1\right]^{-1} \frac{\pi^2 d_p^3 E(m_i)}{\lambda_i}\, dN_p, \tag{13}$$

where $p(N_p)$ is the distribution function of the aggregate size. In Eq. (13) the soot particle temperature T corresponds to the solution of Eq. (1) obtained at a laser fluence F_0 (in mJ/mm^2) and aggregate size N_p. This assumes that the primary particles diameters are monodisperse. Treatment of the distribution of primary particle diameters is not considered in this study. Two aggregate size distribution functions are considered: one is the log-normal distribution function and the other is the δ-function distribution (monodisperse aggregates). The log-normal distribution function is given as

$$p(N_p) = \frac{1}{N_p\sqrt{2\pi}\ln\sigma_g}\exp\left[-\left(\frac{\ln(N_p/N_g)}{\sqrt{2}\ln\sigma_g}\right)\right], \tag{14}$$

where N_g and σ_g are the two parameters of the log-normal distribution function and represent respectively the geometric mean aggregate size and the geometric standard deviation. The mean aggregate size $\bar{N}_p$ (the first moment of the distribution function) is related to the two parameters

through $\bar{N}_p = N_g \exp[0.5(\ln \sigma_g)^2]$. In order to make meaningful comparison between the results of the log-normal distribution and the δ-function distribution, the δ-function is chosen as $p(N_p) = \delta(N_p - \bar{N}_p)$, i.e. it peaks at the geometric mean aggregate size $\bar{N}_p$ of the log-normal distribution. A series of solutions for a range of aggregate sizes are first obtained by solving Eq. (1). These solutions serve as a database for the integration in Eq. (13). The theoretical effective particle temperature T_e is defined such that it satisfies the following expression:

$$\frac{TEI_1}{TEI_2} = \frac{E(m_1)}{\lambda_1^6} \frac{\lambda_2^6}{E(m_2)} \frac{\exp(hc/k_B\lambda_2 T_e) - 1}{\exp(hc/k_B\lambda_1 T_e) - 1}, \tag{15}$$

which is effectively the principle of the two-wavelength optical pyrometer. Substitution of Eq. (13) into Eq. (15) and using the approximation $\exp(hc/\kappa\lambda T) \gg 1$ lead to

$$T_e = \frac{hc}{k_B}\left(\frac{1}{\lambda_2} - \frac{1}{\lambda_1}\right) \Bigg/ \ln \frac{\int_1^\infty p(N_p) N_p \exp(-hc/k_B\lambda_1 T)\, dN_p}{\int_1^\infty p(N_p) N_p \exp(-hc/k_B\lambda_2 T)\, dN_p}. \tag{16}$$

Unlike the experimentally derived particle effective temperature, the theoretical effective particle temperature is independent of the soot absorption functions at the two detection wavelengths λ_1 and λ_2. However, it is strongly dependent on the soot absorption function at the wavelength of the laser [13]. It can also be observed from Eq. (16) that the effective particle temperature derived from the ratio of thermal emission intensities at two wavelengths λ_1 and λ_2, in general, only slightly depends on the values of the two wavelengths.

3. Results and discussion

The transient energy equation (Eq. (1)) was solved using a first-order explicit difference scheme with a variable time step. A very small time step of 0.2 ns was used during and shortly after the laser pulse (up to 50 ns) to resolve the rapid variation of particle temperature. Larger time steps were used after the laser pulse due to slower particle temperature variation. In the calculations of laser-heated soot particles in a laminar diffusion flame the time steps after the laser pulse were 1 ns (between 50 and 100 ns) and 2 ns (after 100 ns). Even smaller time steps of 0.4 ns (between 50 and 100 ns) and 0.6 ns (after 100 ns) were used in the calculations of laser-heated carbon-black particles initially at room temperature (300 K) due to a faster particle temperature decay in this case. Temperature-dependent thermal properties such as the thermal conductivity, the specific heat ratio, the mean free path, the Eucken factor, and the specific heat of soot were used. In all the calculations conducted here, the thermal properties of the surrounding gas were assumed to be the same as those of air. The ambient pressure was 1 atm. The density of soot particle was taken to be 1.9 g/cm^3 and the specific heat of soot was assumed to be the same as that of graphite. The soot absorption function $E(m)$ at 1064 nm (0.4) and the thermal accommodation coefficient of soot particle α (0.37) were taken from our recent study [13]. The spatial profile of the laser is assumed uniform. The temporal profile of the laser power, corresponding to a laser fluence of 1 mJ/mm^2 (the integration of the curve yields 1 mJ), used in the present calculations is shown in Fig. 1. Eq. (1) was solved for 140 aggregate sizes in the range of 1–3000 with non-uniform intervals.

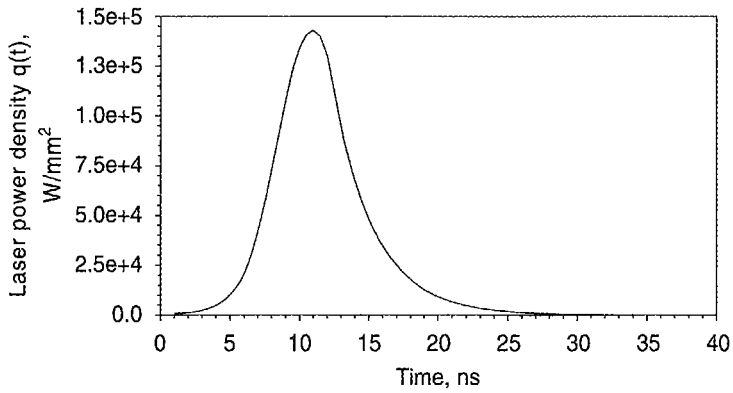

Fig. 1. Temporal profile of the laser power at a laser fluence of 1 mJ/mm^2.

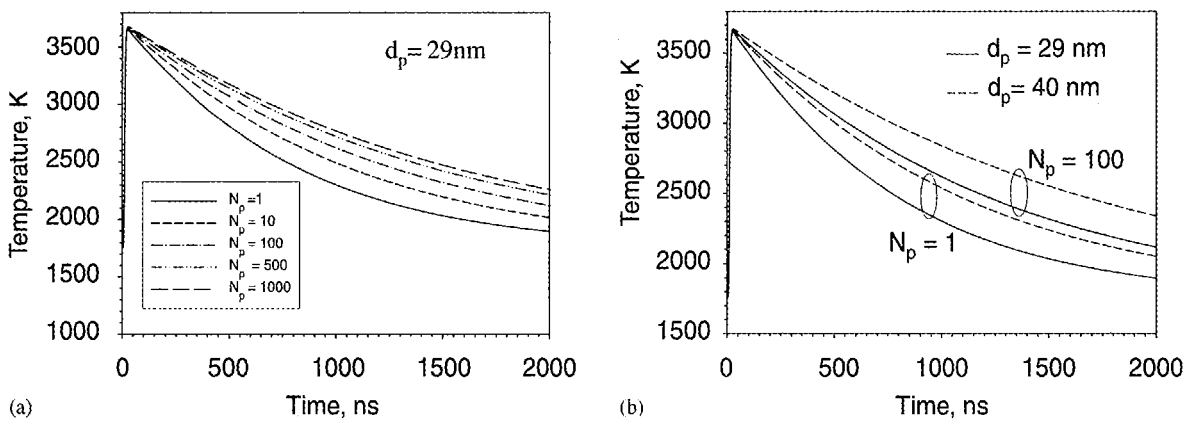

Fig. 2. (a and b) Effects of the aggregate size and the primary soot particle diameter on the soot particle temperature history in the flame case.

These solutions were then used in the numerical evaluation of the integrations in Eq. (16) using a simple trapezoidal algorithm.

3.1. Pulsed laser-heated soot particles in a laminar diffusion flame

The conditions specified in this case correspond to those at 42 mm above the burner exit on the centerline of a laminar coflow ethylene/air diffusion flame described in our previous study [13]. The gas temperature and the primary soot particle diameter are 1750 K and 29 nm, respectively. The laser fluence F_0 used in the calculation of this case is 1.15 mJ/mm^2, which results in a peak particle temperature of about 3660 K. Histories of the soot particle temperature for different single aggregate sizes and primary particle diameters are compared in Fig. 2. The temperature of soot particles in smaller aggregates decays faster than that of particles in larger aggregates due to the shielding effect, which effectively reduces the surface area-to-volume ratio of larger aggregates. The shielding effect is significant for smaller aggregates and becomes progressively

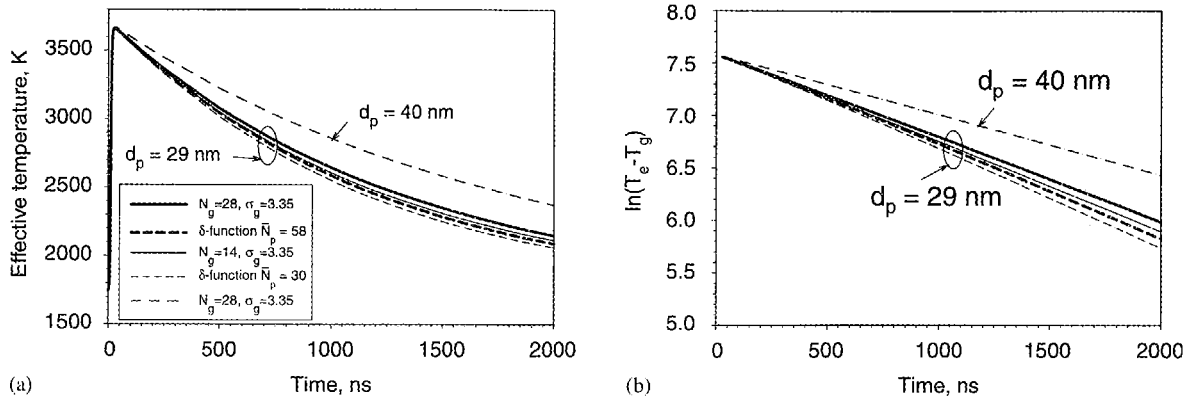

Fig. 3. (a and b) Histories of the effective particle temperature of different aggregate size distributions in the flame case.

less significant for very large aggregates. The peak particle temperature is only slightly dependent on the primary particle diameter d_p and the aggregate size N_p. This is attributed to the following two facts. First, the rate of laser energy absorption by soot particles dominates the rate of heat loss by conduction during the laser pulse. Secondly, both the internal energy and laser energy absorption of soot particles are volumetric processes and the particle diameter effect is cancelled out. The temperature of particles with the smaller primary particle diameter decays faster than that of the larger primary particle, again, because the smaller particle has a larger surface area-to-volume ratio. Results shown in Fig. 2 indicate that the particle temperature decay rate is more sensitive to d_p than N_p.

The effective particle temperature histories calculated for four different aggregate size distributions (two log-normal and two δ functions) and $d_p = 29$ nm are compared in Fig. 3(a). Also shown in Fig. 3 is the effective particle temperature of a larger primary soot particle of $d_p = 40$ nm with a log-normal distribution of aggregate sizes. It is seen that the decay rate of the effective particle temperature depends strongly on the primary particle diameter. Results for $d_p = 29$ nm indicate that the effective particle temperature is relatively insensitive to the aggregate size distribution functions in that they have the same mean aggregate size (compare the thick solid line and the thick dashed line, or the thin solid line and the thin dashed line). Furthermore, a detailed knowledge of the mean aggregate size turns out to be unnecessary in this case since the temperature decay is only slightly dependent on the mean aggregate size (compare the thick solid line and the thin solid line). Therefore, in this flame case the experimental effective temperature decay rate measured using two-color optical pyrometry may be used to estimate the primary particle diameter provided that some estimate of the mean aggregate size is available. When the results shown in Fig. 3(a) are plotted in terms of $\ln(T_e - T_g)$, Fig. 3(b), they all exhibit a nearly linear decay, i.e. temperature decays almost exponentially with time.

3.2. Pulsed laser-heated carbon black particles

The carbon black particles are assumed to have the same thermal properties as soot particles. The particles are initially at 300 K. A higher laser fluence of 1.8 mJ/mm^2 was used in the calculations to achieve a peak particle temperature of about 3650 K. Histories of the carbon black

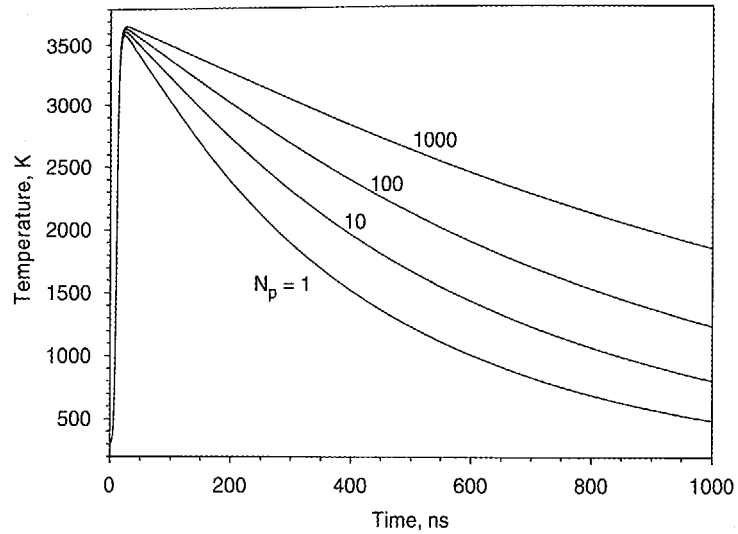

Fig. 4. Effects of the aggregate size on the soot particle temperature history in the carbon black case.

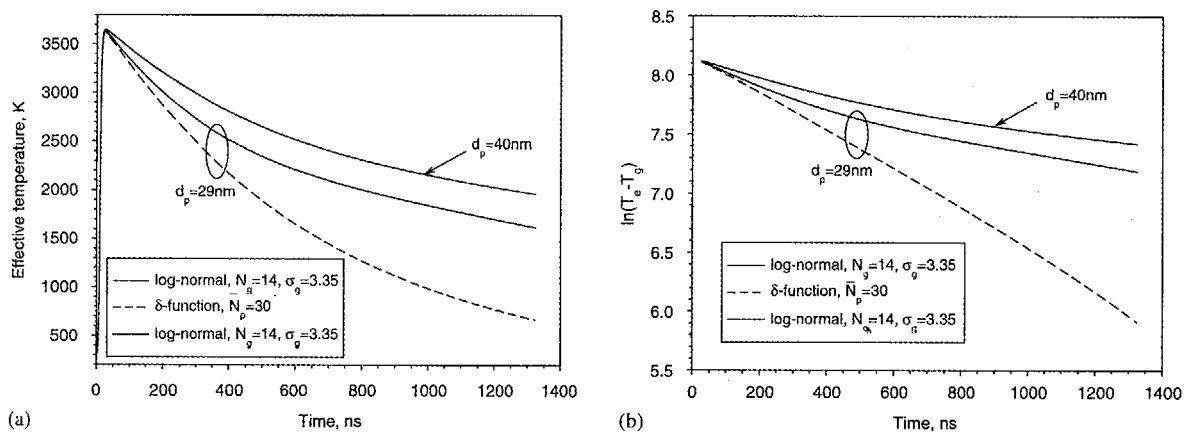

Fig. 5. (a and b) Histories of the effective soot particle temperature of different aggregate size distributions in the carbon black case.

particles ($d_p = 29$ nm) in aggregates of different sizes are compared in Fig. 4. Compared to the results of the flame case shown in Fig. 2, the difference in temperature history between the large and small aggregates is much more significant. The peak particle temperature in the carbon black case is also somewhat more sensitive to the aggregate size compared to the flame case, with the peak particle temperature increasing slightly with the aggregate size. This is due to the higher conduction heat loss rate experienced by particles in smaller aggregates near the end of the laser pulse.

The effective particle temperatures of two different d_p and two different aggregate size distribution functions are compared in Fig. 5. It is evident that the effective particle temperature is strongly dependent on both the primary particle size and the aggregate size distribution function.

Clearly the temporal decay curves of the effective particle temperatures of log-normal distributed aggregates exhibit significant non-linearity, while the decay curve of the monodisperse aggregates (δ-function distribution) is still quite linear, Fig. 5(b). The much slower decay of the effective particle temperature of the log-normal distributed aggregates is due to the significant contribution from the tail of the log-normal distribution where the aggregate sizes are very large and their temperatures are much higher, though they have very small distribution probability. Physically, the thermal radiation intensity from the particles in the laser probe volume at later times is dominated by a small number of very hot and very large aggregates.

Unlike in the flame case, where an approximation of the mean aggregate size seemed sufficient to estimate the primary particle diameter based on the temporal decay curve of the effective particle temperature, a detailed knowledge of the aggregate size distribution is required in the carbon black case for determining the primary particle diameter using the temporal decay curve of the effective particle temperature. In other words, the experimental effective particle temperature decay curve alone cannot differentiate non-aggregated large particles from large aggregates formed by small primary particles.

4. Conclusions

The aggregate based heat transfer model for calculation of nanosecond-pulsed laser-heated soot particle temperature was improved by incorporating the Fuch's approach for heat conduction between the aggregates and the surrounding gas in the transition regime. Effects of the primary particle diameter, aggregate size, and the aggregate size distribution on the particle temperature were investigated in a laminar diffusion flame and in carbon black particles initially at room temperature. For monodisperse aggregates, the particle temperature depends on both the aggregate size and the primary particle diameter. For polydisperse aggregates, the effective particle temperature depends primarily on the primary particle diameter and only slightly on the mean aggregate size and the aggregate size distribution function in the flame case where the ambient gas temperature is relatively high. An approximation of the mean aggregate size is adequate to determine the primary particle diameter in flames based on an experimentally measured effective particle temperature using two-color optical pyrometry. In the carbon black case where the ambient gas temperature is low, the effective particle temperature depends strongly on both the primary particle diameter and the distribution function of aggregate size. The temporal decay rate of soot particle temperature alone is insufficient to determine the primary soot particle diameter.

References

[1] Santoro RJ, Semerjian HG, Dobbins RA. Soot particle measurements in diffusion flames. Combust Flame 1983;51:203–18.

[2] Köylü ÜÖ, Faeth GM. Optical properties of soot in buoyant laminar diffusion flames. J Heat Transfer 1994;116:971–9.

[3] Dobbins RA, Megaridis CM. Morphology of flame-generated soot as determined by thermophoretic sampling. Langmuir 1987;3:254–9.
[4] Quay B, Lee T-W, Ni T, Santoro RJ. Spatially resolved measurements of soot volume fraction using laser-induced incandescence. Combust Flame 1994;97:384–92.
[5] Vander Wal RL, Weiland KJ. Laser-induced incandescence: development and characterization towards a measurement of soot-volume fraction. Appl Phys B 1994;59:445–52.
[6] Shaddix CR, Smyth KC. Laser-induced incandescence measurements of soot production in steady and flickering methane, propane, and ethylene diffusion flames. Combust Flame 1996;107:418–52.
[7] Snelling DR, Smallwood GJ, Campbell IG, Medlock JE, Gülder ÖL. AGARD 90th symposium of the propulsion and energetics panel on advanced non-intrusive instrumentation for propulsion engines. Brussels: Belgium; 1997.
[8] Snelling DR, Smallwood GJ, Sawchuk RA, Neill WS, Gareau D, Clavel D, Chippior WL, Liu, F, Gülder ÖL, Bachalo WD. In-situ real-time characterization of particulate emissions from a diesel engine exhaust by laser-induced incandescence. SAE Paper 2000-01-1994, 2000.
[9] Eckbreth AC. Effects of laser-modulated particulate incandescence on raman scattering diagnostics. J Appl Phys 1977;48(11):4473–9.
[10] Snelling DR, Liu F, Smallwood GJ, Gülder ÖL. Evaluation of the nanoscale heat and mass transfer model of LII: prediction of the excitation intensity, NHTC2000-12132. Proceedings of NHTC'00, 34th National Heat Transfer Conference. Pittsburgh, PA, 2000.
[11] Michelsen HA. Understanding and predicting the temporal response of laser-induced incandescence from carbonaceous particles. J Chem Phys 2003;118(15):7012–45.
[12] Smallwood GJ, Snelling DR, Liu F, Gülder ÖL. Clouds over soot evaporation: errors in modeling laser-induced incandescence of soot. J Heat Transfer 2001;123(4):814–8.
[13] Snelling DR, Liu F, Smallwood GJ, Gülder ÖL. Determination of the soot absorption function and thermal accommodation coefficient using low-fluence LII in a laminar coflow ethylene diffusion flame. Combust Flame 2004;136:180–90.
[14] Hofeldt DL, Real-time soot concentration measurement technique for engine exhaust streams. SAE technical paper series 930079, 1993, p. 33–45.
[15] Faeth GM, Köylü ÜÖ. Soot morphology and optical properties in nonpremixed turbulent flame environments. Combust Sci Tech 1995;108:207–29.
[16] Köylü ÜÖ, Faeth GM, Farias TL, Carvalho MG. Fractal and projected structure properties of soot aggregates. Combust Flame 1995;100:621–33.
[17] Brasil AM, Farias TL, Carvalho MG. A receipt for image characterization of fractal-like aggregates. J Aerosol Sci 1999;30(10):1379–89.
[18] Köylü ÜÖ, Xing YC, Rosner DE. Fractal morphology analysis of combustion-generated aggregates using angular light scattering and electron microscope images. Langmuir 1995;11:4848–54.
[19] Filippov AV, Rosner DE. Energy transfer between an aerosol particle and gas at high temperature ratios in the knudsen transition regime. Int J Heat Mass Transfer 2000;43:127–38.
[20] McCoy BJ, Cha CY. Transport phenomena in the rarefied gas transition regime. Chem Eng Sci 1974;29:381–8.
[21] Chapman S, Cowling TG, The mathematical theory of non-uniform gases. 3rd ed. Cambridge: Cambridge University Press; 1970. p. 249.